blood®
Regular Article

THROMBOSIS AND HEMOSTASIS

Metabolites in a mouse cancer model enhance venous thrombogenicity through the aryl hydrocarbon receptor–tissue factor axis

Mostafa Belghasem,[1] Daniel Roth,[1] Sean Richards,[2] Marc Arthur Napolene,[2] Joshua Walker,[2] Wenqing Yin,[2] Nkiruka Arinze,[3] Chimera Lyle,[2] Cheryl Spencer,[1] Jean M. Francis,[2] Cristal Thompson,[2,4] Christopher Andry,[1] Stephen A. Whelan,[5] Norman Lee,[5] Katya Ravid,[2,4] and Vipul C. Chitalia[2,6,7]

[1]Department of Pathology and Laboratory Medicine and [2]Department of Medicine, Boston University School of Medicine, Boston, MA; [3]Department of Surgery, Boston University Medical Center, Boston, MA; [4]Whitaker Cardiovascular Institute, Boston University School of Medicine, Boston, MA; [5]Chemical Instrumentation Center, Boston University, Boston, MA; [6]Veterans Affairs Boston Healthcare System, Boston, MA; and [7]Global Co-Creation Labs, Institute of Medical Engineering and Science, Massachusetts Institute of Technology, Cambridge, MA

KEY POINTS

- VTE is the second most common cause of noncancer-related deaths in patients with malignancy, yet its mechanisms remain poorly defined.
- Increased tryptophan metabolites in a colon cancer model activated the AHR TF/PAI-1 axis in the venous wall to induce thrombosis.

Patients with malignancy are at 4- to 7-fold higher risk of venous thromboembolism (VTE), a potentially fatal, yet preventable complication. Although general mechanisms of thrombosis are enhanced in these patients, malignancy-specific triggers and their therapeutic implication remain poorly understood. Here we examined a colon cancer–specific VTE model and probed a set of metabolites with prothrombotic propensity in the inferior vena cava (IVC) ligation model. Athymic mice injected with human colon adenocarcinoma cells exhibited significantly higher IVC clot weights, a biological readout of venous thrombogenicity, compared with the control mice. Targeted metabolomics analysis of plasma of mice revealed an increase in the blood levels of kynurenine and indoxyl sulfate (tryptophan metabolites) in xenograft-bearing mice, which correlated positively with the increase in the IVC clot size. These metabolites are ligands of aryl hydrocarbon receptor (AHR) signaling. Accordingly, plasma from the xenograft-bearing mice activated the AHR pathway and augmented tissue factor (TF) and plasminogen activator inhibitor 1 (PAI-1) levels in venous endothelial cells in an AHR-dependent manner. Consistent with these findings, the endothelium from the IVC of xenograft-bearing animals revealed nuclear AHR and upregulated TF and PAI-1 expression, telltale signs of an activated AHR-TF/PAI-1 axis. Importantly, pharmacological inhibition of AHR activity suppressed TF and PAI-1 expression in endothelial cells of the IVC and reduced clot weights in both kynurenine-injected and xenograft-bearing mice. Together, these data show dysregulated tryptophan metabolites in a mouse cancer model, and they reveal a novel link between these metabolites and the control of the AHR-TF/PAI-1 axis and VTE in cancer. (*Blood*. 2019;134(26):2399-2413)

Introduction

Malignancy induces a highly thrombogenic milieu, which manifests clinically as deep vein thrombosis (DVT) and pulmonary embolism. Both of these events fall under the category of venous thromboembolism (VTE).[1] Current estimates suggest that 20% to 30% of VTEs are associated with cancer.[2] Large epidemiological studies have shown that VTE occurs in 4% to 7% of hospitalized cancer patients.[3,4] The incidence of VTE varies with tumor type. The National Hospital Discharge Survey found that the highest incidence of VTE occurs in patients hospitalized with pancreatic cancer and brain tumors.[5] Also, gastrointestinal cancers confer a high risk of VTE, increasing the odds of VTE by 20-fold (odds ratio, 20.3; 95% confidence interval: 4.9-83.0).[6] VTE in patients with cancer can be a potentially fatal event. Khorana et al[7] examined causes of death in 4466 cancer patients at 117 US centers. A vast majority of deaths (70.9%) were ascribed to the progression of underlying cancer. Among noncancer-related deaths, thrombotic events were one of the leading contributors (9.2%), of which VTE was the cause of death in 33% of these patients.

Several cancer, host, and therapy-related factors contribute to VTE pathogenesis and are used to estimate the risk of VTE in different prediction models.[1] The risk of VTE increases with the stage of cancer. Cancer stage defined according to Tumor, Nodes and Metastasis (TNM) classification takes into account overall tumor burden and metastatic disease. Chemotherapy increases the risk of VTE by 6.5-fold compared with patients not

receiving chemotherapy. Although subclinical activation of prothrombotic pathways is implicated in cancer-associated VTE, the cancer milieu reflects an imbalance of prothrombotic and antithrombotic factors. A host of mediators released from tumor cells, including pro-inflammatory cytokines, mucinous glycoproteins, and microparticles, contributes to the prothrombotic component. Of this, increased tissue factor (TF), a potent trigger of the extrinsic coagulation cascade, is a well-established mediator of cancer-associated VTE. Accordingly, high TF-expressing tumors, such as brain and pancreatic cancer, exhibit increased levels of TF in the blood, and these patients are at the highest risk of VTE.[8] Although TF enhances thrombogenesis, thrombolytic/fibrinolytic pathways are suppressed in patients with malignancy by mediators such as plasminogen activator inhibitor 1 (PAI-1).[9]

Emerging evidence implicates specific metabolites contributing to thrombosis in chronic kidney disease,[10-14] which is uniquely characterized by the retention of several metabolites. Of these, tryptophan metabolites are highly prothrombotic[10-12,15] and have been further categorized as such in 2 independent human cohorts.[13] Retained metabolites include kynurenine (Kyn) and indoxyl sulfate (IS), which bind to aryl hydrocarbon receptor (AHR) to induce its nuclear translocation.[15] Nuclear AHR activates transcription of the *TF* gene in endothelial cells[12] and increases the release of TF-bearing microparticles in the circulation. In vascular smooth muscle cells (vSMCs), AHR activation protects TF protein from ubiquitination and proteasomal degradation.[10-12,13,15] Collectively, these data showed that AHR activation upregulated TF expression in both endothelial cells and vSMCs to augment thrombosis. Interestingly, inhibitors of thrombolysis are also regulated by the AHR pathway. For example, the *PAI-1* gene is a direct target of AHR and is induced by AHR activation in hepatoma cells.[16,17] Although the AHR pathway is a well-established, xenobiotic, and chemical carcinogenic pathway,[18] the aforementioned evidence points to the role of AHR in controlling thrombosis.

The AHR-TF axis warrants investigation in cancer-associated VTE because the blood levels of metabolites such as Kyn are increased in a wide variety of cancers,[19-27] including colon cancers.[23,24] With this rationale, the current study investigated a colon cancer–specific VTE model to probe the role of cancer-associated tryptophan metabolites in regulating the AHR-TF prothrombotic axis.

Methods

Xenograft model

All the animal experiments were approved by the Institutional Animal Care and Use Committee at Boston University (AN# 15449). A group of animals consisting of an equal proportion of male and female athymic nude mice (catalog #002019; The Jackson Laboratory, Bar Harbor, ME) were used. The average weights of the male and female athymic mice were 29.3 ± 5.9 g and 23.6 ± 3.9 g, respectively. The mice were fed a normal chow diet and water ad libitum. HT-29 cells, a human colorectal adenocarcinoma cell line with epithelial morphology purchased from ATCC (Manassas, VA), were grown in RPMI-1640 medium (Thermo Fisher Scientific, Waltham, MA) with 10% fetal bovine serum and 1% penicillin streptomycin. The cells were trypsinized and resuspended in a 1:1 mixture of serum-free media and growth factor–poor Matrigel (Corning Inc., Tewksbury, MA). HT-29 at a concentration of 1×10^6 cells in 200 μL of suspension was injected into the subcutaneous tissue on the backs of mice using a 23-gauge needle.

A caliper (VWR International, Radnor, PA) was used to measure tumor size weekly for 4 consecutive weeks. The tumors were measured along their longest axis (L) and the axis perpendicular to the long axis (W). Tumor volume (V) was calculated by using the equation $L \times (W^2) = V$.[28] Although the caliper assessment is important to track the growth of xenografts injected subcutaneously and is performed by a single examiner to avoid interpersonal errors in this study, we acknowledge a possible limitation concerning precise measurement. However, the focus of this study was on the functional association between levels of tumor-secreted metabolites and thrombosis. The identity of the tumor as colon cancer was confirmed by staining tissue for β-catenin, a well-established mediator central to the colon cancer pathogenesis. Colon cancer is characterized by activation of Wnt signaling and nuclear β-catenin.

Inferior vena cava ligation model

The overall strategy of the venous thrombosis model in cancer (Figure 1A) is similar to one described previously.[9,29,30] After 4 weeks of tumor growth, mice underwent inferior vena cava (IVC) ligation in addition to ligation of the left gonadal vein and nearby tributaries, as previously described.[31] Briefly, under isoflurane anesthesia, a midline laparotomy was performed. A length of 6-0 silk suture was threaded between the vessels to ligate the IVC. The IVC was ligated distal to the renal veins. All tributaries nearby the IVC were also ligated to create a total stasis environment within the IVC for induction of thrombus formation. Mice with sham injections served as experimental controls. After 48 hours of IVC ligation, the clots were carefully removed from the vessel wall and weighed.

For a Kyn-mediated thrombosis model, Kyn (catalog #K8625; MilliporeSigma, Burlington, MA) dissolved in phosphate-buffered saline was injected intraperitoneally (IP) daily at 100 mg/kg body weight, with or without CH223191 (catalog #C8124; MilliporeSigma) 10 mg/kg[11,15] IP once daily between 7:30 and 8:30 AM for 4 days before IVC ligation. Essentially, there was close to a 9- to 10-hour gap between the injections. The treatment was continued for 48 hours until clot harvest.

For the HT-29 thrombosis model, mice received CH223191 as noted earlier[11,15] for 5 days before IVC ligation and was continued until clot harvest. During the course of the experiments depicted in this article, 6 mice died after IVC ligation.

Targeted metabolomics

Blood samples (40-50 μL) from facial bleeds were collected before the IVC ligation procedure, pipetted into 1.5 mL tubes containing heparin, and placed into a centrifuge at 2000*g* for 30 minutes to separate the plasma. The plasma was stored at −80°C before processing. Media collected from cultured HT-29 cells in the presence or absence of serum and/or tryptophan (as indicated in the Results section) were analyzed for Kyn release. The Metabolomics Service Center at the Chemical Instrumentation Center, Boston University, analyzed the samples for Kyn and IS levels, as we have previously described.[32]

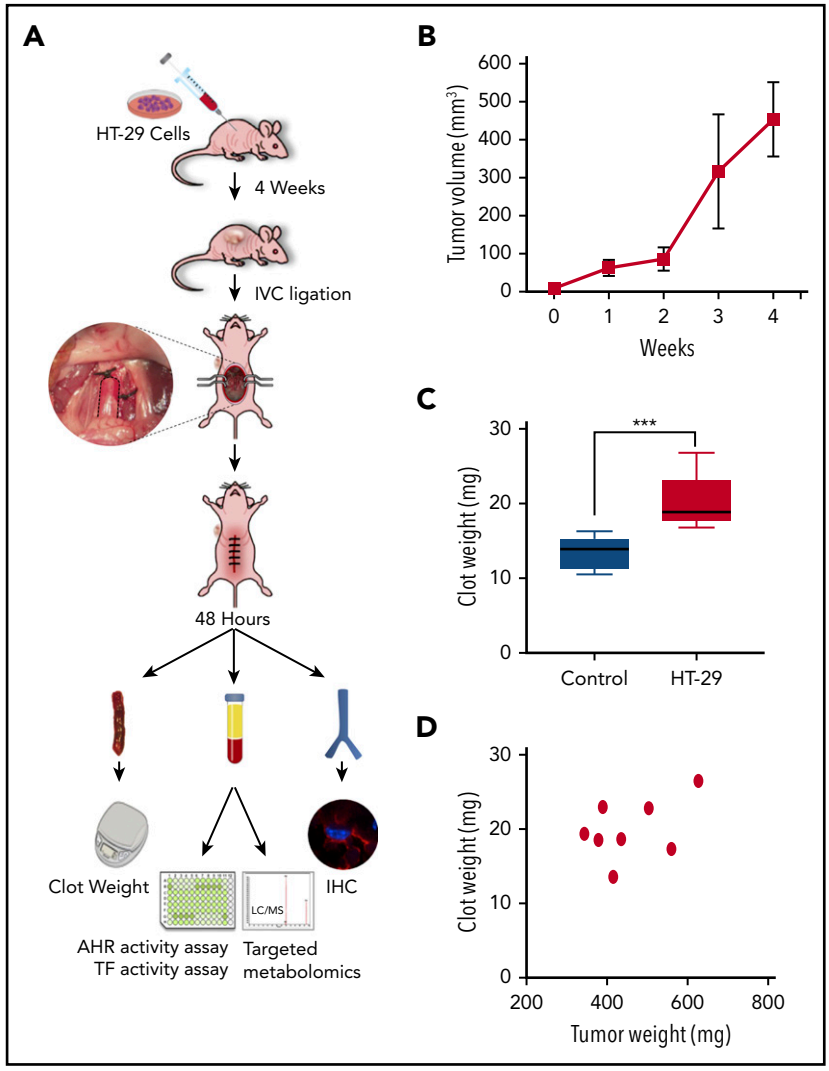

Figure 1. Generation of a venous thrombosis model of colon cancer. (A) Schema of the experimental model. Athymic nude mice were injected with HT-29 cells, and the xenograft was allowed to grow for 4 weeks. IVCs were ligated, and after 2 days, the animals were euthanized for harvest of the xenograft and clot. Blood collected was examined for targeted metabolomics, AHR, and TF activity assays. (B) Tumor xenograft growth. A group of 8- to 10-week-old athymic female (n = 4) and male (n = 4) mice were injected subcutaneously with HT-29 cells suspended in Matrigel (N = 8). An average tumor volume is shown. Error bars = SEM. A Student *t* test was applied. Compared with the tumor volume at time 0, $P = .003$ for the tumor volumes at week 2 and 3 and $P < .001$ at week 4. (C) Increase in clot weight of mice bearing colon cancer xenografts. Box plots of the clot weights of mice depicted in panel B and the controls (without xenografts) are shown. The lines in the boxes represent median levels, and the lower and upper boundaries of the boxes represent the 25th and 75th percentiles, respectively. The lower and upper whiskers represent the minimum and maximum values. ***$P = .001$. (D) Tumor volume at the end of harvest was correlated with the clot weight. N = 8 mice. Pearson's correlation $R^2 = 0.21$ and $P = .25$.

Cell culture and immunoblotting

Human umbilical vein endothelial cells were obtained from Lonza (Basel, Switzerland) and cultured in 5% carbon dioxide incubators according to the manufacturer's instructions, as previously described.[13] Immunoblots were performed as described elsewhere.[11]

Immunohistochemistry and immunofluorescence

For immunohistochemistry (IHC) and immunofluorescence (IF), the tissue was harvested, sectioned (5 μm), and fixed in formaldehyde or paraformaldehyde, respectively, using conventional procedures. Specifically for IHC, the slides were deparaffinized and rehydrated. Antigen retrieval was performed by using a prewarmed 10 mM trisodium citrate solution with 0.05% Tween 20 buffered to pH 6.0. A microwave was used to heat the slides in the trisodium citrate buffer at 95°C for 20 minutes. The slides were then permeabilized in a solution of 0.3% Triton X-100 in 1× phosphate-buffered saline for 10 minutes, and subjected to IHC as previously described.[11,15] The antibodies used for IHC were mouse monoclonal anti-AHR (incubated at 1:50 dilution for overnight hours at 4°C) (MA1-514; Thermo Fisher Scientific) and rabbit polyclonal anti–β-catenin (incubated at 1:50 dilution for 2 hours at room temperature; sc-7199; Santa Cruz Biotechnology, Dallas, TX). For immunoblots of PAI-1, we used rabbit anti–PAI-1 antibody from Cell Signaling Technology (catalog #1190; Danvers, MA) at 1:1000 dilution incubated overnight at 4°C. For IF, a mouse monoclonal antibody from Abcam (ab-125687; Cambridge, United Kingdom) was used at 1:100 dilution, incubated overnight at 4°C. These antibodies were raised by using a synthetic peptide corresponding to the residues surrounding Arg294 of human PAI-1 protein (recognizes mouse, human, and baboon PAI-1), and mouse PAI-1 (recognizes mouse PAI-1). For TF studies, we used a prevalidated rat anti-mouse anti-TF antibody from Genentech (South San Francisco, CA; 1H1) at 1:100 to 1:1000 dilution, incubated overnight at 4°C, as previously described.[11] This antibody has been used by other groups for immunoblot and IF detection of TF.[33,34] For CD31, a rabbit polyclonal anti-CD31 antibody (catalog #ab28364; Abcam) validated for immunoblots and IF (1:1000 and 1:100 at overnight at 4°C) was used. This antibody is known to react against mouse, human, and pig CD31. For IF, the secondary antibodies consisted of Alex Fluor 488, 594, and 647 (Molecular Probes, Eugene, OR) at 1:250 dilution for 45 minutes at room temperature. Smooth muscle cells were marked with anti–α smooth muscle actin antibody (catalog #ab5694; Abcam).

For image quantification, the entire slide was scanned by a motorized stage system using the Nikon NIS Elements software

at the Boston University School of Medicine (BUSM) Imaging Core. The images were processed in ImageJ (National Institutes of Health, Bethesda, MD), where the signal was converted to grayscale, and the number and intensity of pixel were analyzed as integrated density by using plugin Fiji. The area of vein was marked as the region of interest. The integrated density of all the images was normalized to its area.

Luciferase assay

Plasma from these animals was also used for the luciferase assay. The assay was performed by using the immortalized human umbilical vein endothelial cells, as previously described.[13,15]

Surface procoagulant TF activity assay

Human umbilical vein endothelial cells were used for the intact cell surface procoagulant TF activity assay, as previously described.[13,15]

Statistical analysis

Summary statistics are presented as the mean, median and standard deviation (SD) or standard error of the mean (SEM), 25th or 75th percentile, or the entire range of values, including minimum and maximum value as appropriate. A Student *t* test, analysis of variance, Pearson's correlation analysis, and Wilcoxon rank sum test were performed as appropriate. Statistical significance was assessed at the $P < .05$ level.

Results

A xenograft model using HT-29 cells, a validated tumorigenic cell line,[28] was generated in athymic nude mice (Figure 1A). In a group of male and female athymic mice injected with HT-29 cells, the xenografts grew rapidly between 3 and 4 weeks' postinjection. At the end of 4 weeks, the tumors reached an average volume of 452.66 mm^3 (SEM ± 32.41 mm^3) (Figure 1B). No difference in tumor volume was noted between the 2 sexes. The colon cancer cells in this xenograft were authenticated by using β-catenin, an oncogenic marker important for the growth of colon cancer.[28] A histological analysis of the xenografts revealed a compact mass of tumor cells and interstitium (supplemental Figure 1A, available on the *Blood* Web site). The expression of β-catenin was readily observed in the cytosol and nuclei of colon cancer cells (supplemental Figure 1B); none was observed in the interstitium, as β-catenin is an epithelial tumor marker.

Having validated the growth of colon cancer xenografts, we next examined thrombogenicity in these animals by performing an IVC ligation at 4 weeks after tumor inoculation (Figure 1A). This is a model of acute complete venous thrombosis driven by stasis-induced venous wall injury and enhanced TF expression in endothelial cells.[31] The clots were harvested 48 hours after IVC ligation. The control group consisted of animals without a xenograft. Clot weight served as a biological readout of venous thrombogenicity. Our results revealed an 80% increase in clot weight in mice with HT-29 (mean ± SEM, 20.26 ± 1.31 mg) compared with control mice (11.33 ± 0.05 mg; $P = .001$) (Figure 1C), and no differences were noted between the 2 sexes. These results confirmed enhanced venous thrombogenicity in the presence of a colon cancer xenograft. We then examined the relationship between the clot weight and tumor mass. No correlation was observed between them, suggesting that after a rapid growth phase, factors other than the volume of the primary tumor may influence venous thrombogenicity (Figure 1D).

Previous study samples have shown that tryptophan metabolites, such as IS and Kyn, exert prothrombotic properties in both mice and humans.[11-13,15,35] Considering a possible accelerated tryptophan metabolism of cancer cells, these metabolites were quantified by using a prevalidated liquid chromatography–mass spectrometry (LC/MS) method.[32] The results showed a 3-fold increase in plasma Kyn levels in HT-29 xenograft animals compared with control animals (control, 0.29 ± 0.026 μg/mL; HT-29, 0.68 ± 0.15 μg/mL; $P < .001$) (Figure 2A). Plasma concentrations of IS were 2-fold higher in animals with xenografts (control, 0.89 ± 0.09 μg/mL; HT-29, 1.60 ± 0.33 μg/mL; $P = .03$) (Figure 2B). Because these metabolites are known to augment thrombosis,[10-14] we posited that the levels of these metabolites are likely to correlate with clot burden. Our analysis showed a linear correlation between the levels of Kyn, IS, and the clot weight (Figure 2C-D), with positive Pearson R^2 values of 0.78 for Kyn and 0.48 for IS. Although these data suggest a stronger correlation between Kyn and clot weight, compared with IS, it supports their potential causality in inducing venous thrombogenicity, which was probed further.

The source of Kyn in the xenograft-bearing mice could be endogenous and/or released by HT-29 cells. To ascertain the later possibility, both basal production of Kyn and one induced by serum were examined in cultured HT-29 cells. We posited that the generation of Kyn is likely to increase with supplementation of medium with tryptophan (substrate) or by serum, which includes tryptophan. To this end, early-passage 1×10^4 HT-29 cells seeded in 12-well plates were serum starved and then treated with or without 10% serum in the presence of 1 mM of tryptophan dissolved in water. The vehicle-treated cells served as controls. The media were harvested after 48 hours of incubation and analyzed by LC/MS, using a method we previously published.[32] The media without exposure to cells (basal medium) were also analyzed, and these values were subtracted from the media exposed to HT-29 cells (Figure 2E).

Our results showed that HT-29 cells generated Kyn in basal conditions and at significantly higher levels with the supplementation of serum or tryptophan. In the serum-free condition, Kyn concentration in the medium was 9.00 ± 1.77 nM (mean ± SEM), which was increased 3-fold (28.82 ± 10.96 nM; $P = .014$) with the addition of tryptophan. Compared with the serum-free condition, the addition of 10% serum increased the Kyn level to 29.40 ± 13.89 nM ($P = .03$). However, supplementation of tryptophan to the medium with 10% serum did not further increase Kyn release. Taken together, these results show that HT-29 cells generate and secrete Kyn in the medium. These results are in line with the observed increase in Kyn levels in the blood of HT-29 xenograft-bearing mice.

Because these metabolites are known to activate TF through the AHR pathway in endothelial cells,[19-22,32] we posited that the plasma of animals with the colon cancer xenograft is likely to have an increased ability to induce AHR and TF activity in endothelial cells. Because DVT occurs on an intact monolayer of endothelial cells of a vein, we used venous endothelial cells for these assays. AHR activity was determined by using human umbilical vein endothelial cells stably expressing an AHR-responsive

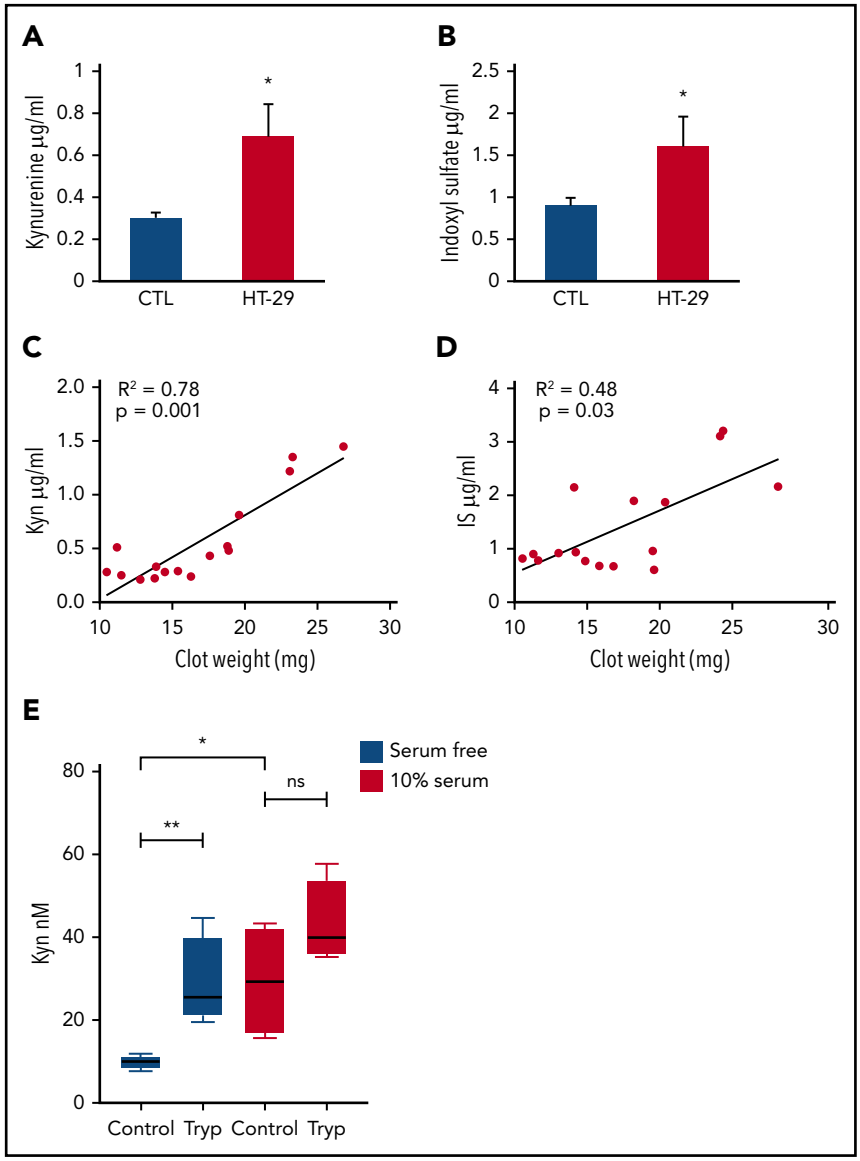

Figure 2. Increase in Kyn and IS in plasma of mice with colon cancer xenografts. (A) Increase in Kyn level in the plasma of animals injected with the colon cancer xenograft. Plasma obtained from athymic mice with HT-29 xenografts (N = 8, as described in Figure 1A) before IVC occlusion were examined for Kyn levels. The uninjected athymic mice served as controls (N = 8). An average of 2 independent determinations in plasma of the mice from Figure 1D is shown. A Student *t* test was performed. Error bars = SEM. $P < .001$. (B) Increased IS in plasma of animals with colon cancer xenografts. Plasma obtained from athymic mice with HT-29 xenografts before IVC occlusion was examined for IS levels as noted earlier. Average of 2 independent determinations in plasma of the mice from Figure 1D is shown. A Student *t* test was performed. Error bars = SEM. $P = .03$. (C) Correlation of Kyn levels with clot weights. Kyn levels recorded in a total of 16 mice from both groups (xenograft-bearing and control, as described in Figure 1A) were correlated with the clot weights. Pearson's correlation analysis was performed. Line represents a linear regression performed to obtain the *P* value. (D) Correlation of IS levels with the clot weight. IS levels obtained from 16 mice from both groups (xenograft-bearing and control) were correlated with clot weights. Pearson's correlation and linear regression analysis were performed. (E) Kyn production by HT-29 cells. HT-29 cells were cultured for 48 hours in the presence or absence of 10% serum and/or tryptophan (Tryp). The harvested media were analyzed for Kyn by using LC/MS, and values were subtracted from the levels in the basal medium (nonsupplemented). The box plots are representative of Kyn levels analyzed in quadruplets. The line within the box corresponds to the median, the borders represent the 25th and 75th percentiles, and the whiskers represent the highest and the lowest values. *$P = .014$ and **$P = .03$. ns, not significant.

promoter tethered to a luciferase reporter.[13,15] AHR activity was measured by using firefly luciferase and normalized to protein content (relative luciferase unit [RLU]). We used 0.5% to 2% concentration of plasma from mice to determine the optimal concentration to be used for AHR activity (Figure 3A). Treatment with 0.5% to 1% plasma resulted in an increase in AHR activity in a linear manner, which was not seen with the plasma concentration >1%. Further investigation was therefore conducted by using 1% plasma.

The plasma from mice with xenografts stimulated significantly greater AHR activity than did the plasma from control animals (control, 8941 ± 935.7 RLU/µg protein; HT-29 xenograft, 20037 ± 3157 RLU/µg protein; $P = .007$) (Figure 3B). Next, a monolayer of human umbilical vein endothelial cells was treated with plasma from mice bearing xenografts, and the cells were subjected to the surface procoagulant TF activity assay. Plasma from xenograft-bearing mice induced a 2-fold increase in TF activity (control, 77.83 ± 10.28 pM/10^3 cells; HT-29 xenograft, 142.3 ± 19.5 pM/10^3 cells [$P = .019$]) (Figure 3C). This increase in TF activity was inhibited in the presence of CH223191, a competitive AHR antagonist[15] (HT-29, 142.3 ± 19.5 pM/10^3 cells; HT-29 with CH223191, 96.50 ± 5.68 pM/10^3 cells [$P = .047$]). These results suggest that the plasma from animals with xenografts activates the AHR pathway and enhances TF activity in an AHR-dependent manner.

PAI-1 is also regulated by the AHR pathway in other cell types.[16,17] We therefore examined if AHR activation increased PAI-1 levels in endothelial cells. To this end, endothelial cells were treated with different concentrations of Kyn with and without the AHR antagonist CH223191. The lysates from these cells showed approximately doubling of PAI-1 expression with Kyn concentrations as low as 0.1 µM, which was substantially suppressed by the 20 µM of the AHR antagonist (Figure 3D). Interestingly, the concentration of Kyn found in the plasma of xenograft-bearing animals (corresponding to an average of 2.8 µM) (Figure 2A) induced PAI-1 expression in endothelial cells. Consistent with this notion, close to a 2-fold upregulation in PAI-1 expression was observed in endothelial cells treated with plasma from xenograft-bearing mice ($P < .001$). The treatment with CH223191 inhibited PAI-1 expression in response to plasma

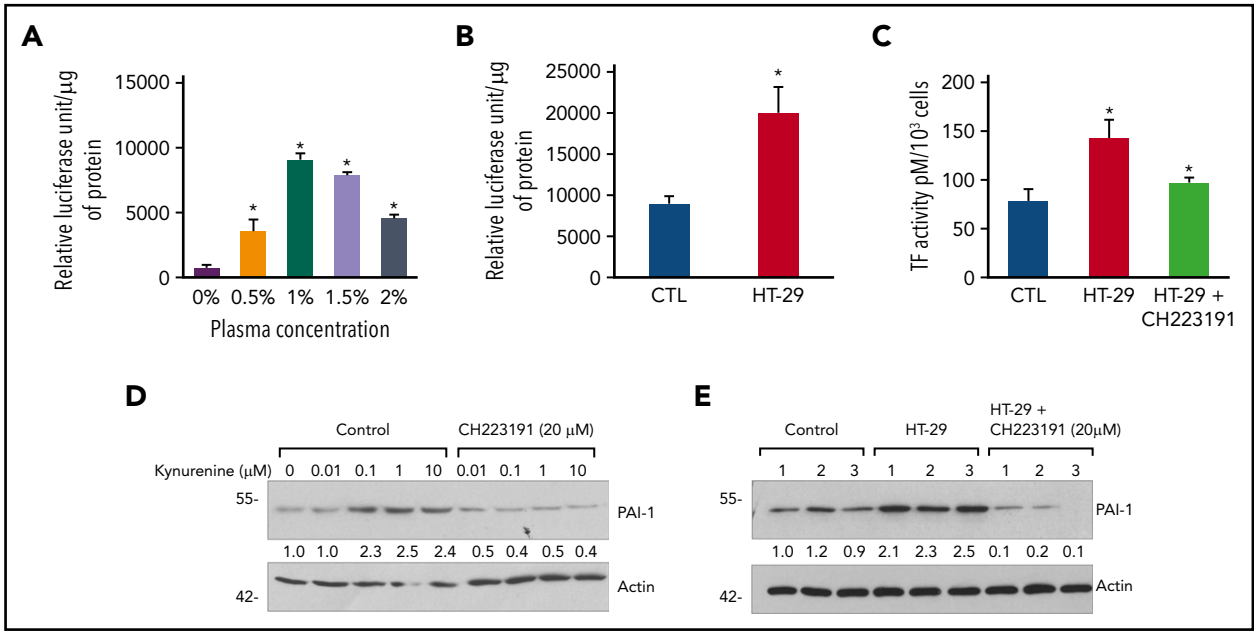

Figure 3. Increased AHR activity and TF and PAI-1 levels in endothelial cells treated with plasma from animals with xenografts. (A) Optimum concentration of mouse plasma for AHR activity. Endothelial cells stably expressing a xenobiotic responsive element promoter-luciferase reporter construct were treated for 24 hours with indicated concentrations of plasma from 3 athymic control mice (without xenograft). AHR activity was quantified by firefly luciferase units and normalized to amount of protein. An average of 3 independent experiments is shown. Error bars = SEM. Compared with cells treated with serum-free medium (control), *P* values were .04, .003, .02, and .03 for plasma concentration of 0.5%, 1%, 1.5%, and 2%, respectively. (B) Higher AHR-inducing activity of plasma from mice with a colon cancer xenograft. AHR activity assay was performed as noted earlier by using 1% plasma obtained from mice with a colon cancer xenograft. An average of 2 independent determinations performed in duplicate is shown. Plasma samples obtained from 8 mice per group as described in Figure 1A were used. Error bars = SEM. *P* = .007 for plasma from xenograft-bearing (HT-29) animals compared with matching controls (CTL). (C) Higher TF-inducing activity of plasma from mice with a colon cancer xenograft. Endothelial cells were treated for 24 hours with 1% plasma obtained from mice with a colon cancer xenograft with or without 20 μM of CH223191. Plasma from animals without tumors served as negative controls as described in Figure 1A. The cells were subjected to procoagulant TF activity assay by using Factor VIII and Factor XIa and chromogenic substrate (see Methods). An average of 2 independent experiments with plasma obtained from 8 animals per group performed in duplicates is shown. Error bars = SEM. **P* = .019 compares CTL and HT-29 and *P* = .047 HT-29 and HT-29 + CH223191. (D) Kyn increases PAI-1 in an AHR-dependent manner. Endothelial cells treated with a titrated concentration of Kyn as shown with or without AHR inhibitor CH223191 for 24 hours. Using western blotting, equal amounts of lysates were probed separately on different blots for PAI-1 and β-actin (loading control) due to the proximity of the molecular weights. Representative immunoblots from 3 independent experiments are shown. Molecular weight ladder (kDa) is shown on the left of the blot. The PAI-1 band normalized to β-actin by using ImageJ is shown, and values obtained are noted below the PAI-1 blot. (E) Endothelial cells treated with 1% plasma from control and HT-29 mice as alluded in Figure 1A with or without 20 μM of CH223191 for 24 hours. The lysates from 3 separate representative mice are shown from a total 8 mice per group. Actin served as a loading control.

from both the control and xenograft-bearing mice (*P* = .001 and *P* < .001, respectively) (Figure 3E; supplemental Figure 2). However, the extent of PAI-1 suppression was greater in cells treated with plasma from xenograft-bearing mice, compared with cells treated with plasma from control mice. This can be explained by the heightened AHR activity in xenograft-bearing mice (Figure 3B) for the antagonist to suppress, as observed in other disease models.[15] Because PAI-1 inhibits thrombolysis, its upregulation in venous endothelial cells is consistent with the higher clot burden observed in animals with xenografts.

Collectively, the aforementioned data indicated that animals with colon cancer xenografts, which are known AHR agonists, had elevated blood levels of IS and Kyn. Therefore, we posited that AHR signaling is likely activated in endothelial cells of the IVC in xenograft-bearing mice, which will upregulate AHR's downstream mediators, namely TF and PAI-1. Using nuclear localization of AHR as an evidence of AHR activation,[18] the IVCs of animals exposed to xenografts for 4 weeks were compared with those of control mice (not bearing xenografts). In these experiments, mice did not undergo IVC ligation to avoid the confounding effect of surgical trauma on endothelial protein expression (Figure 4A). CD31 antibody was used to confirm their identity as endothelial cells. The IVC endothelial cells of control mice revealed AHR predominantly localized in the cytosol, whereas the IVC endothelial cells of HT-29–injected mice revealed AHR localized in the nucleus (Figure 4B). Minimal nuclear AHR localization in control IVC endothelium can be ascribed to the presence of known endogenous AHR ligands. We examined the percentage of cells positive for nuclear AHR from an equal number of $CD31^+$ endothelial cells surveyed in 24 images of IVC per each experimental group. Of the endothelial cell lining in IVC, 5.2 ± 1.62% of endothelial cells in control mice were positive for nuclear AHR; xenograft-bearing mice had a 2.5-fold higher percentage of AHR-positive endothelial cells (13.17 ± 3.04%; *P* = .025). These results suggested a heightened state of AHR activation within the endothelial layer of the IVC of xenograft-bearing mice.

We next probed the downstream targets of AHR (TF and PAI-1) in the IVC of xenograft-bearing mice that did not undergo IVC ligation. Minimal TF expression was observed in the control mice (Figure 5A-B**)**. Compared with control mice, expression of TF and PAI-1 was 4.5-fold and 2.5-fold higher, respectively, in the IVCs of xenograft-bearing mice (*P* = .032 and *P* = .0425).

The IVC lysates probed by immunoblotting includes endothelial cells and vSMCs, in which AHR activation by solutes is known to upregulate TF and augment thrombosis.[10,11,13,15] Although DVTs in humans occur on the largely intact endothelial layer,[36] that is

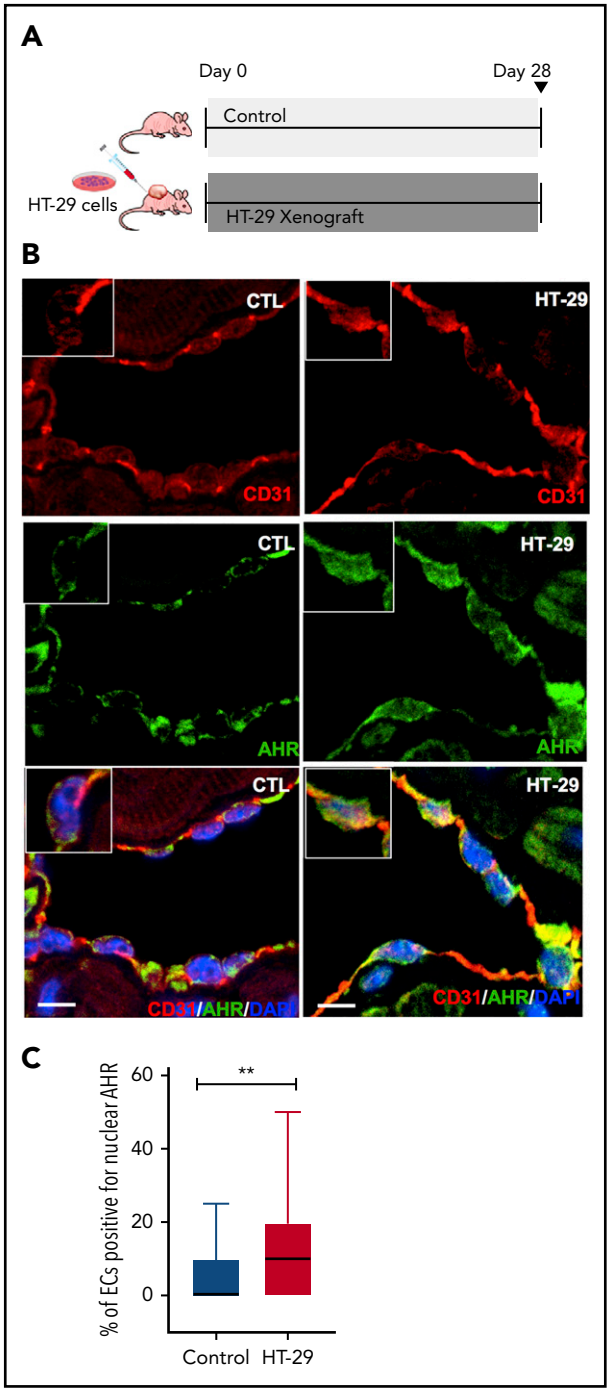

Figure 4. Increased activation of AHR in IVC of animals with colon cancer xenografts. (A) Experimental design. A group of 8- to 10-week-old (total 8 mice, 4 mice of each sex) athymic mice were injected with HT-29 cells. Mice without HT-29 with the same sex distribution served as controls. At the end of 4 weeks, the xenograft volumes in these mice were 418.19 ± 26.93 mm^3 (in the same range as those in Figure 1B). No IVC ligation was performed in these groups. (B) AHR status in the IVC of mice with colon cancer xenografts. IVCs harvested from control (CTL) and colon cancer xenograft-bearing mice (HT-29) were stained with prevalidated anti-AHR[16] and anti-CD31 antibodies and imaged by using confocal microscopy. Alexa Fluor secondary antibodies were used. 4′,6-Diamidino-2-phenylindole (DAPI) was used for nuclear stain. Representative images from a segment IVC of 8 animals analyzed per group are shown. The inserts show a representative endothelial cell with AHR in cytosol and in the nucleus. Scale bar = 10 μm. (C) The IVC of xenograft-bearing mice contained a higher percentage of endothelial cells with nuclear AHR. Each group consisted of 8 IVCs from a total of 8 mice in each experimental group: males (n = 4) and females (n = 4). One section of IVC was examined per mouse. Three high-power

not the case in the IVC occlusion model in mice, which is known to inflict severe vessel wall injury and drive TF from different cell types within the vessel wall.[37] We therefore examined TF expression in endothelial cells, marked with anti-CD31 (Figure 5C) and in vSMCs, identified by α smooth muscle actin staining (asterisk in Figure 5C and supplemental Figure 3A) and laser confocal microscopy. For this experiment, IVCs were harvested from mice without ligation to avoid the confounding effect of surgical trauma on TF expression (supplemental Figure 3B). We observed a monolayer of vSMCs consistent with a substantially thinner IVC wall, compared with an aorta. TF expression was evident in endothelial cells and in vSMCs, and both were increased in xenograft-bearing mice. Our further analysis focused on the endothelial layer given its relevance to the human DVT.[36] The endothelial layer was marked as the region of interest, and TF and PAI-1 expression was derived as integrated density by using ImageJ. Both TF and PAI-1 in endothelial cells exhibited significantly higher levels in the xenograft-bearing mice compared with the control mice ($P = .002$ and $P = .009$, respectively) (Figure 5D,F). Taken together, these results suggest that the IVC endothelial cells of mice injected with HT-29 have greater activation of AHR signaling, which upregulates TF and PAI-1 expression. This finding corroborated with the higher venous thrombogenicity observed in xenograft-bearing mice (Figure 1C).

The role of AHR activity in regulating cancer-associated venous thrombosis was further probed by using pharmacological manipulation in 2 discrete mice models. Due to the fact that Kyn levels were elevated in the xenograft-bearing mice, Kyn levels correlated strongly with the clot weight (Figure 2C), and that plasma from these mice induced AHR and TF and PAI-1 levels in endothelial cells (Figure 3), we posited that an AHR antagonist might suppress Kyn-mediated TF and PAI-1 expression in IVC of mice, as well as reduce venous thrombogenicity. As a control experiment, we first examined the effect of AHR inhibition in mice without xenografts. A group of 6 athymic mice were given CH2213191 for 5 days followed by IVC ligation. The injections were continued for 48 hours more after IVC occlusion, until harvest. An equal number of vehicle-treated mice served as controls (Figure 6A). The IVC clot weights in mice treated with CH223191 tended to be lower compared with those of control mice (control mice, 12 ± 0.71 mg tumors; CH223191, 10.44 mg ± 0.56 mg tumors; $P = .112$) (Figure 6B), suggesting no effect of AHR inhibition on venous thrombogenicity in control mice. The effect of the competitive inhibitor is also a function of the levels of agonist ligands in the milieu. Plasma from xenograft-bearing mice contained significantly higher levels of the AHR agonists Kyn and IS (Figure 2). It stands to reason that CH223191 will likely exhibit greater effect in the Kyn-injected or xenograft-bearing mice compared with control mice with lower levels of AHR agonistic ligands (Kyn and IS) in the circulation (Figure 2A-B).

We next investigated whether the AHR inhibitor suppressed Kyn-mediated venous thrombogenicity. In this experiment, a group of 8- to 10-week-old athymic female and male mice were

Figure 4 (continued) field images, randomly obtained, were analyzed by using a laser confocal microscope. In essence, 24 images per group were examined and presented as percentage of endothelial cells positive for nuclear AHR. $^{**}P = .025$.

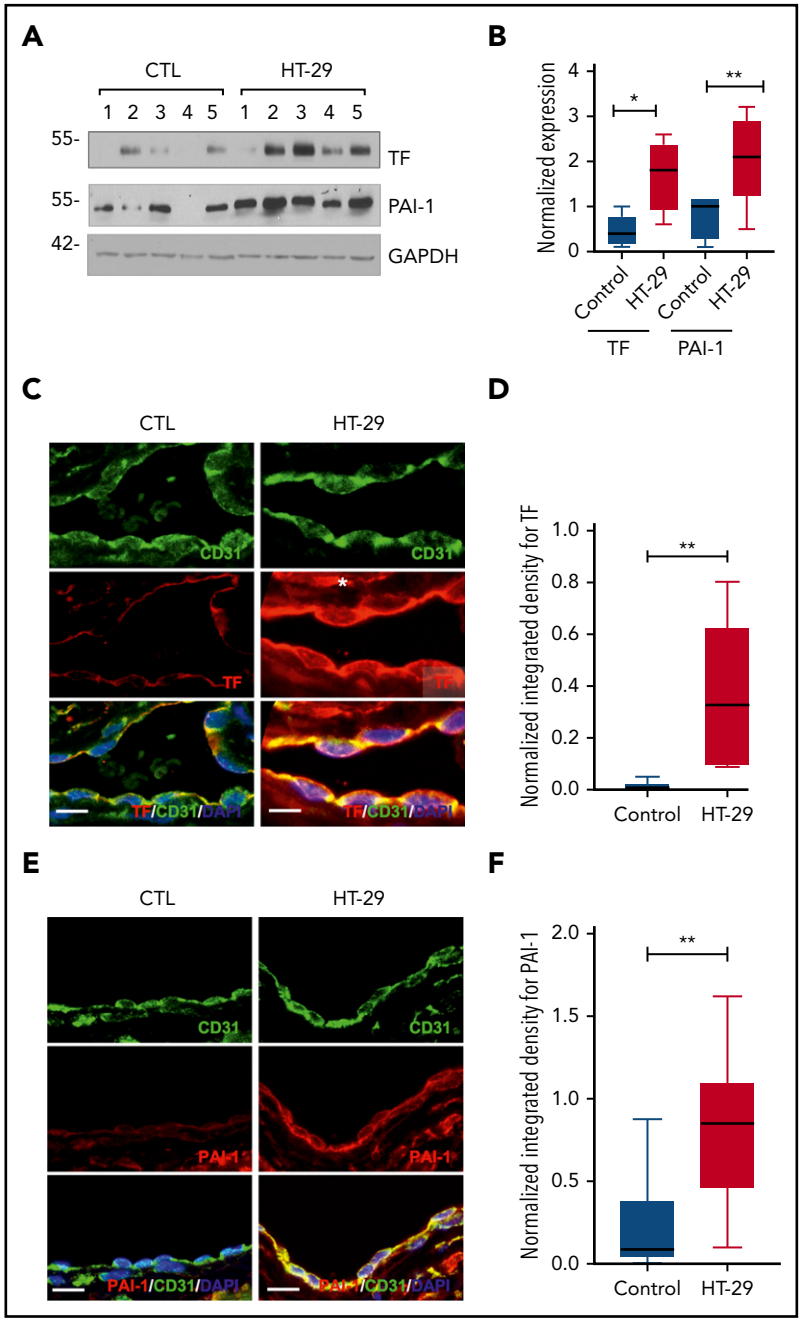

Figure 5. Increased TF and PAI-1 in the IVC of animals with colon cancer xenografts. (A) IVC from mice shown in Figure 4A were harvested, divided for immunoblotting, and fixed for immunofluorescence microscopy. Of 8 mice per group, the lysates from 5 mice were resolved on sodium dodecyl sulfate–polyacrylamide gel electrophoresis gels due to sufficient quantity of protein in these samples. Equal amounts of samples were separately probed on different western blots with the indicated antibodies (owing to proximity of bands). Glyceraldehyde-3-phosphate dehydrogenase (GAPDH) served as a loading control. (B) The immunoblot bands of TF and PAI-1 shown in Figure 4A were normalized to GAPDH in the aforementioned gel. Normalized TF and PAI-1 from control and HT-29 mice are shown on box plots. Asterisks (* and **) compare the expression of TF and PAI-1, respectively, between the 2 groups. *P = .032 and **P = .0425. (C) Increased expression of TF in the IVC of animals with colon cancer xenografts. IVC from animals with a xenograft without IVC ligation were stained by using anti-TF and anti-CD31 antibodies. Alexa Fluor secondary antibodies were used. 4′,6-Diamidino-2-phenylindole (DAPI) was used for nuclear stain. Un-injected animals served as controls (CTL). Images are representative of IVCs from 8 mice in each group. Scale bar = 10 μm. (D) Three images per IVC were analyzed, and a region of interest was marked corresponding to the endothelial cells. Integrated density was normalized to the surface area of the region of interest measured in microns by using ImageJ. Data are presented as a box plot, and the Student t test was used to compare the 2 groups. **P = .002. (E) Increased expression of PAI-1 in the IVC of animals with colon cancer xenografts. IVCs from animals with xenografts without IVC ligation, as described earlier, were stained by using anti–PAI-1 and anti-CD31 antibodies. Images are representative from 8 mice in each group. Scale bar = 30 μm. (F) Integrated density for PAI-1 was performed as noted earlier. The data are presented as a box plot, and the Student t test was used to compare the 2 groups (**P = .009).

injected with Kyn, with or without CH223191 (Figure 6C). Mice not receiving Kyn injections served as a control. One-way analysis of variance showed a significant overall difference in clot weights between the 3 groups (P = .02). Further comparison of the groups by using the Student t test revealed that mice injected with Kyn exhibited a significantly higher clot weight (18.55 ± 1.34 mg) compared with that of control mice (11.03 ± 0.7 mg; P = .02) (Figure 6D). The treatment of mice with the AHR antagonist reduced clot weight in both control and Kyn + CH223191 animals to baseline, leaving no statistically significant difference between the experimental groups (10.61 ± 0.19 mg; P = .03).

These observations strongly suggested that the AHR antagonist lowered Kyn-mediated hyper-thrombogenicity to baseline. This reduction was also reflected in alterations in the levels of TF and PAI-1 in the IVC lysates of Kyn-injected mice (supplemental Figure 4; Figure 6D). Compared with the control mice, Kyn exposure significantly increased both TF (2.0 ± 0.22-fold; P = .03) and PAI-1 (1.82 ± 0.04-fold; P = .02) expression, both of which were suppressed by CH223191 (TF, P = .04; PAI-1, P = .01). No significant difference was noted in TF and PAI-1 expression between control mice (Figure 6E) and Kyn + CH223191–injected mice, suggesting that the AHR inhibitor normalized the Kyn-induced increase in expression of TF and PAI-1 within the vessel wall.

This experiment implicates a Kyn–AHR axis in modulating IVC thrombosis. To confirm the hypothesis that AHR suppression inhibits venous thrombogenicity, further functional assays were

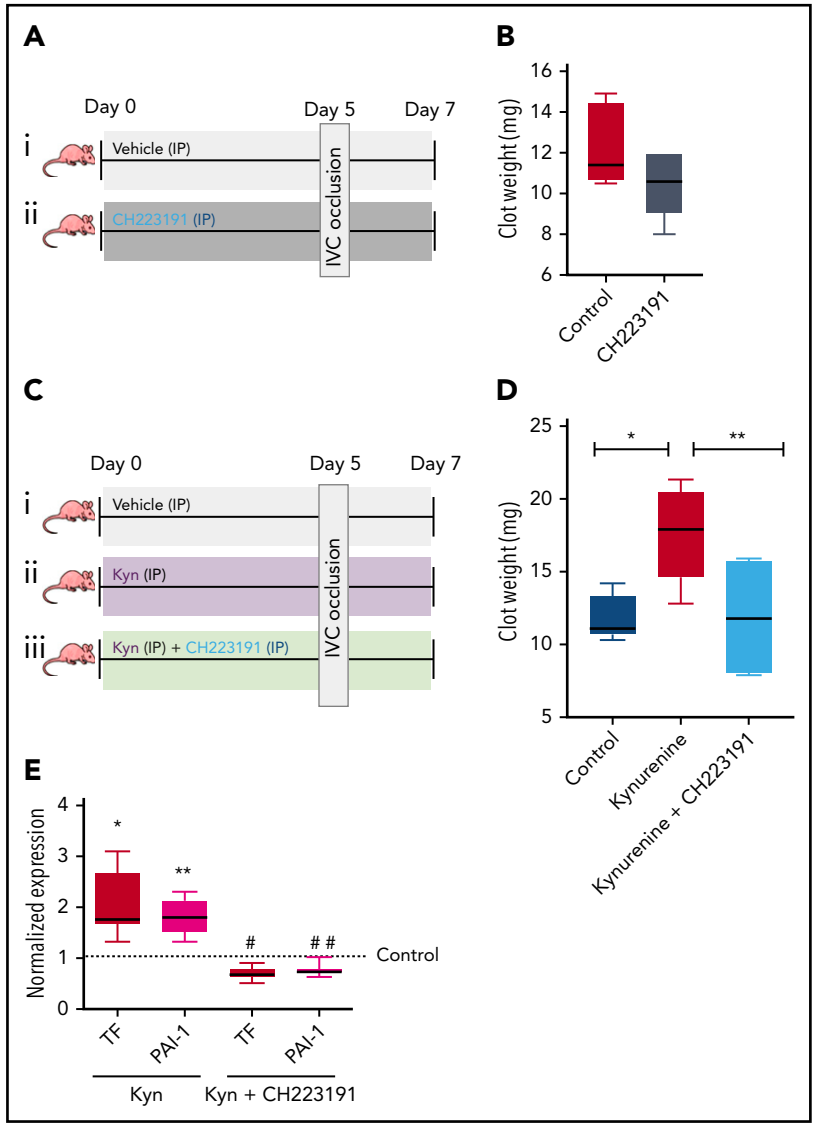

Figure 6. Kyn-mediated venous thrombogenicity and TF and PAI-1 are suppressed by AHR inhibition. (A) Experimental design. A group of 12 mice (6 male mice and 6 female mice) were divided into 2 equal groups, with 3 male mice given 10 mg/kg CH2213191 or vehicle (used as control), and similarly, 3 female mice given 10 mg/kg CH2213191 or vehicle. The treatment was continued for 2 more days after IVC ligation. The clots from mice harvested after 48 hours following surgery were weighed. (B) IVC clot weights are presented as a box plot for each group. $P = .112$ compares control and CH223191-treated groups. (C) Scheme examining AHR inhibition in Kyn-mediated venous thrombosis. A group of 8- to 12-week-old athymic mice consisting of an equal proportion of male and female animals was injected IP with 100 mg/kg Kyn with or without 10 mg/kg CH223191, once daily before the procedure. Vehicle-treated mice served as a control group. The animals were subjected to the IVC ligation, and clots were harvested 48 hours after ligation. Control group, n = 6 mice; Kyn group, n = 8 mice; and Kyn + CH223191 group, n = 6 mice. (D) IVC clot weights presented as a box plot for each group from panel C. $*P = .02$ compares the control and Kyn groups, and $**P = .03$ compares the Kyn and Kyn + CH223191 groups. (E) TF and PAI-1 expression from each mouse was normalized to glyceraldehyde-3-phosphate dehydrogenase. Changes in the TF and PAI-1 expression (as measured by western blotting) compared with the controls (the dotted line) of mice from panel C are shown. The borders of the box depict 25th and 75th percentiles, and whiskers correspond to minimum and maximum values. The number of mice is listed in panel A. Student *t* tests were performed. Compared with the control mice, $*P = .02$, $**P = .04$. Compared with the Kyn-injected mice, $\#P = .03$ and $\#\#P = .01$. No significant difference was noted in TF and PAI-1 between the control and Kyn + CH223191 groups.

performed. We injected a group of xenograft-bearing mice (equal proportion of male and female mice) with HT-29 cells. After 3 weeks, the mice were randomly divided into 2 groups: first group was injected with 10 mg/kg IP of CH223191 once daily until the harvest of clots, and the second group was injected with the vehicle (control group) in the same manner (Figure 7A). Tumor volume and sera samples were collected from these mice after euthanasia. Comparison of sample analysis from both the groups revealed no differences in the tumor volumes or Kyn levels (Figure 7B-C). However, the IVC clot weights showed a 4-fold reduction with CH223191 treatment. The mean clot weight in HT-29 mice was 16.68 ± 5.69 mg; in the HT-29 + CH223191 group, it was 4.56 ± 2.93 mg ($P = .001$) (Figure 7D).

A parallel experiment was performed in which the IVCs were harvested after 4 weeks of xenograft growth to examine the expressions of TF and PAI-1 in IVC using IF and immunoblotting. These mice did not undergo IVC occlusion to avoid the confounding effect of surgical trauma on TF and PAI-1 expression. Compared with the control groups, IVC lysates from mice treated with CH223191 exhibited 6-fold and 4-fold reductions in the levels of TF and PAI-1, respectively (both, $P = .001$) (Figure 7E-F). Because the lysates of IVC consisted of proteins from non–endothelial cell types, IF microscopy was performed to specifically examine the changes in TF and PAI-1 in the endothelial cells of IVC. The IVCs without surgical manipulation were fixed and stained for TF, PAI-1, and CD31, and their expressions were quantitated as integrated density (Figure 8). Compared with the HT-29 mice, the IVC endothelial cells of mice treated with CH223191 revealed a significant suppression of both TF ($P = .005$) and PAI-1 ($P < .001$). These data all suggest that AHR inhibition in xenograft-bearing mice is responsible for suppression of TF and PAI-1 expression in the endothelial cells and reduction of IVC clot weight, suggesting that AHR inhibition leads to reduced venous thrombogenicity.

Discussion

Leveraging a colon cancer–specific DVT model, the current study demonstrated a previously unrecognized connection between colon cancer–associated increases in certain metabolites and the resulting regulation of factors that contribute to cancer-associated VTE. Our results showed that animals with

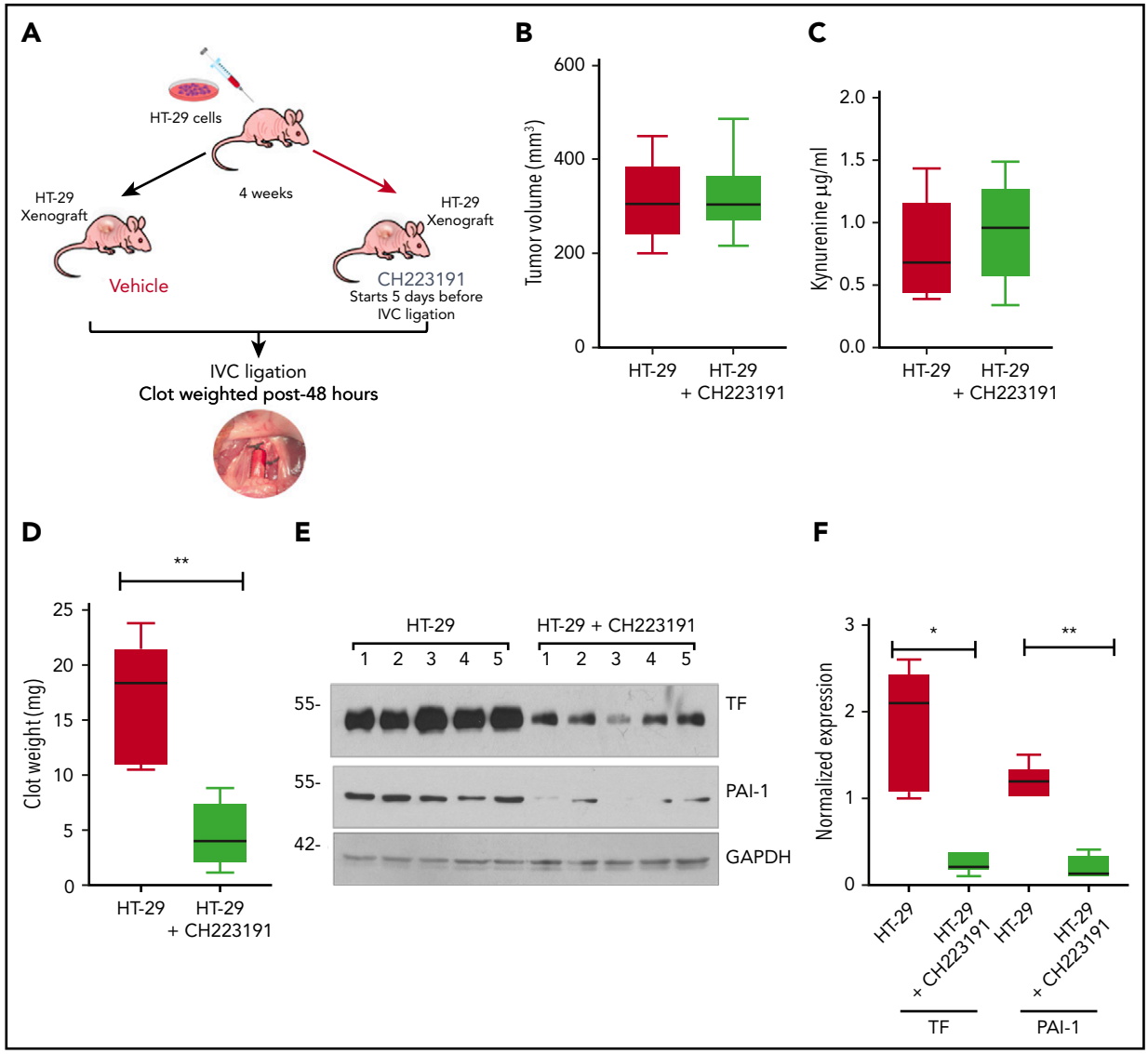

Figure 7. Enhanced venous thrombogenicity in an HT-29–induced cancer model is abrogated by AHR inhibition. (A) Experimental design. An equal number of male and female athymic mice (N = 10) were injected with HT-29 and after 3 weeks randomized to 2 subgroups (N = 5 per group). HT-29 group had 3 male and 2 female mice and HT-29 + CH223191 had 2 male mice and 3 female mice. Mice were given CH223191 IP for a total of 7 days until the harvest of IVC clots. The group treated with the vehicle (dimethyl sulfoxide) served as controls. (B) Tumor volumes at the end of 4 weeks after cell injection are presented as box plots, $P = .878$. (C) Kyn levels in plasma of mice at the time of harvest are shown in box plots, $P = .235$. (D) IVC clots from both the groups as in Figure 6A are shown in box plots. The Student *t* test was used to compare the groups. $^{**}P = .001$. (E) IVCs harvested from mice, as in Figure 6A from a parallel experiment without the IVC ligation surgery, were lysed and probed separately for TF and PAI-1. Equal amounts of lysates were used in each blot, and glyceraldehyde-3-phosphate dehydrogenase (GAPDH) served as a loading control. The numbers at the top correspond to 5 separate mice used for the study. (F) TF and PAI-1 normalized to GAPDH for both groups, N = 5 per group represented as box plots. A Student *t* test was used to compare TF and PAI-2 separately between the groups. $^{*}P = .001$ for TF and $^{**}P = .001$ for PAI-1 and compares the HT-29 vs the HT-29 + CH223191 group.

colon cancer xenografts have increased blood levels of Kyn and IS, which induce AHR activity in the endothelial cells of large veins. This action results in upregulation of TF and PAI-1 expression. TF is a known trigger for thrombogenesis through the extrinsic coagulation cascade, and PAI-1 is known to inhibit thrombolysis, both of which in concert may augment the clot burden culminating in DVT, as illustrated in Figure 9. Furthering our understanding of the pathogenesis of cancer-associated VTE, this research supports the metabolite AHR-TF/PAI-1 axis as a potential contributor to this condition. The nodes of this axis are quantifiable and can be further leveraged to stratify human cancer patients at risk of VTE, as performed for other disease models.[13] The translational potential of this prothrombotic axis is further underscored by the fact that both AHR and TF are therapeutically targetable proteins, and tryptophan metabolites might be modulated by dietary interventions.

Increase in prothrombotic metabolites in cancer

Blood levels of Kyn are increased in a wide variety of cancers, such as non–small cell lung cancer, brain, ovarian, pancreatic, gastric, colon, and bladder cancer.[19-27] In 97 patients with colorectal cancer, Engin et al[24] reported a significant rise in blood levels of Kyn to 1.24 nM compared with 0.89 nM in matched cancer-free control subjects. Kyn is the product of tryptophan metabolism, and its generation is regulated by a set of enzymes such as tryptophan dioxygenase tryptophan 2,3-dioxygenase

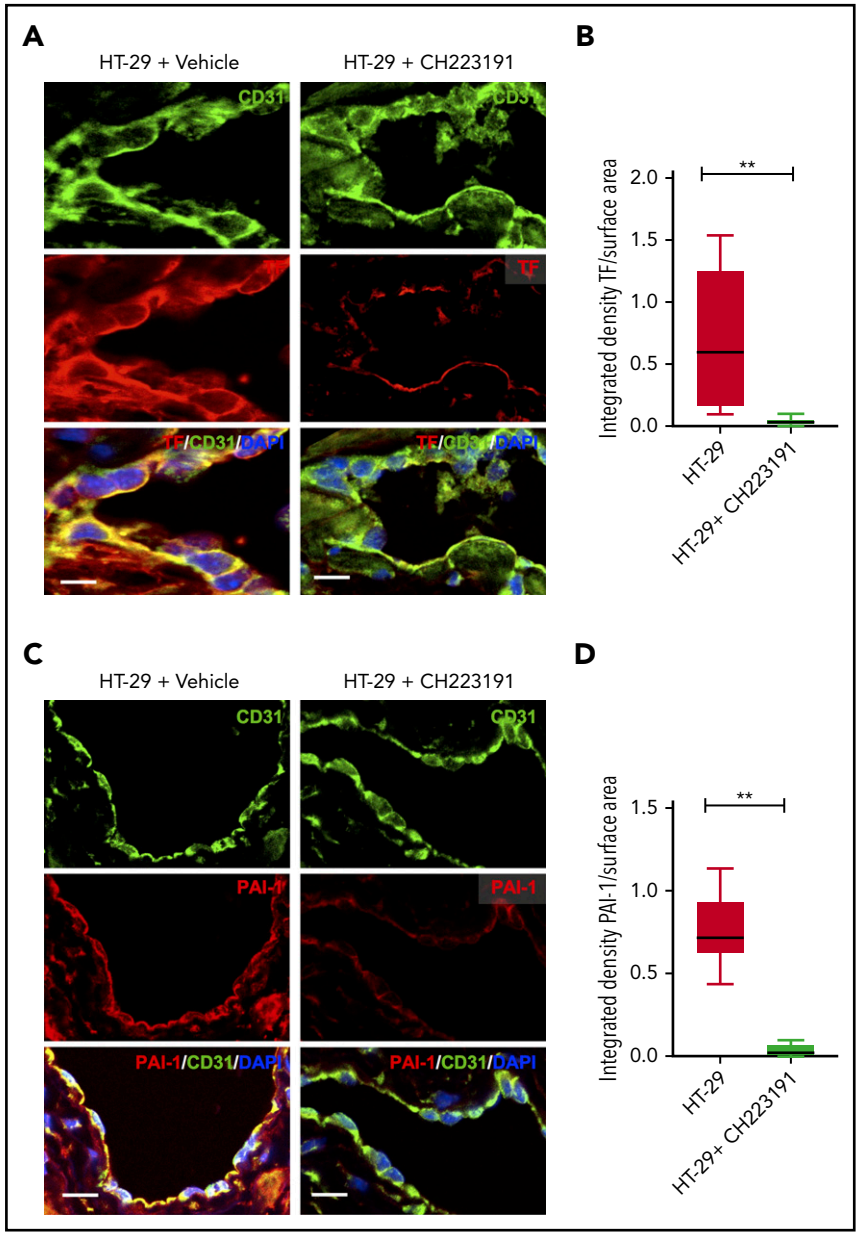

Figure 8. TF and PAI-1 levels in the endothelium of IVC of HT-29–injected mice are suppressed by an AHR antagonist. IVCs of mice were harvested and divided for immunoblotting (as shown in Figure 7E-F) and fixed for immunofluorescence microscopy. (A,C) Immunofluorescence images of IVC stained with anti-TF and anti–PAI-1 along with anti-CD31. The secondary antibodies consisted of Alexa Fluor. Green = CD31; red = TF or PAI-1. 4′,6-Diamidino-2-phenylindole (DAPI) was used to stain the nuclei. Representative images of 5 IVC mice are shown. Scale bar = 10 μm for TF and 30 μm for PAI-1. (B,D). Three images per IVC were analyzed, and a region of interest was marked corresponding to the endothelial cells. Integrated density was normalized to the surface area of the region of interest measured by using ImageJ as microns. The data are represented as box plots, and a Student *t* test was used to compare both the groups, $^{**}P = .005$ for TF and $P < .001$ for PAI-1.

and indoleamine 2,3-dioxygenase 1 that are also present in tumor cells, among other tissues. Colon cancer cells such as HT-29, Caco-2, and LC-180 cells harbor the entire enzyme machinery for tryptophan catabolism, whose rate is several folds higher than that in normal colon epithelium.[38] Qi et al[39] showed that the human colon cancer cells grown in vitro converted tryptophan to Kyn and that the treatment with anticancer agents suppressed the generation of Kyn and resulted in the accumulation of tryptophan within the cancer cells and its milieu. However, such studies performed in a two-dimensional cell culture may not accurately reflect the metabolism of tumors in a three-dimensional structure.[40,41] Nonetheless, our analysis of HT-29 cells suggests that the xenografts of HT-29 used in this study are likely to be the source of increased Kyn levels in the blood of these mice.

An increase in blood levels of IS in the context of a colon cancer xenograft model is intriguing. Although IS is a tryptophan metabolite similar to Kyn, it is generated from indole in the gut microbiome by tryptophanase-containing bacteria.[14] Indole is further converted to IS in the liver by the cytochrome system. At a steady state, the blood level of IS is a function of its production and excretion through the kidneys. An increase in the blood levels of IS in the setting of colon cancer may suggest higher production, because its renal excretion is less likely to be affected in this xenograft model. It is plausible that the alteration in microbiome with tumor grafting[42] may contribute to the increased levels of IS. Dysbiosis in patients with colon cancer is known[43] and implicated in the growth and progression of colon cancer.[44] Although this observation warrants further exploration, the current results indicate that investigation of the role of gut microbiome and cancer-associated VTE is needed.

Human studies have indicated a heightened risk of cancer-associated VTE with a greater tumor burden, inclusive of tumor mass and stage.[4,45] Intriguingly, the current study revealed

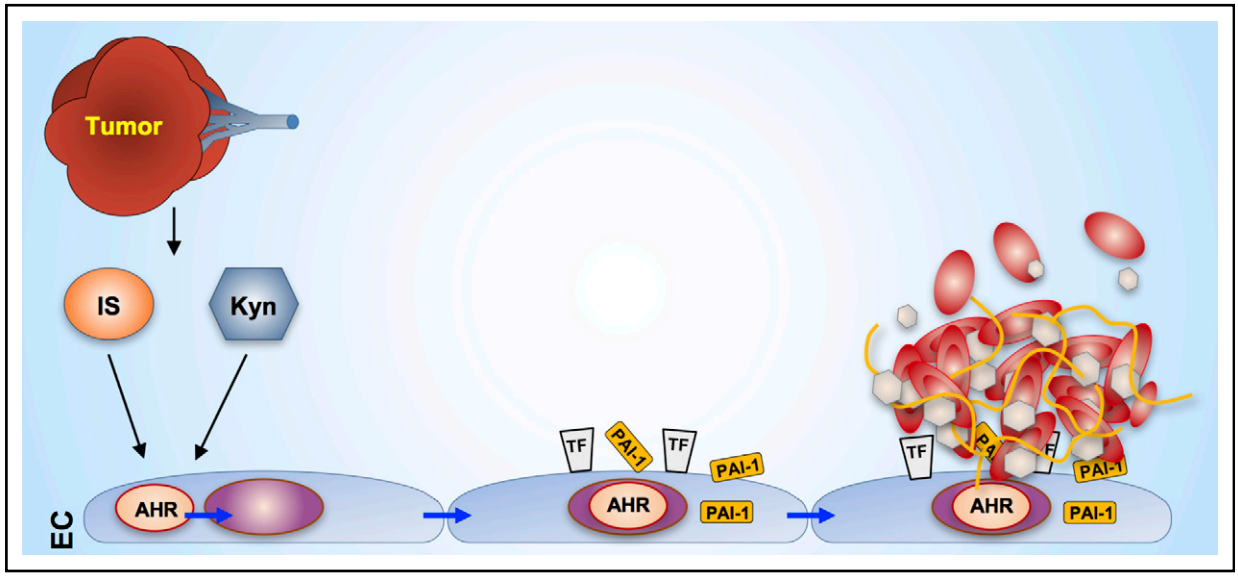

Figure 9. A prothrombotic metabolite AHR-TF/PAI-1 axis is associated with cancer-associated VTE. In animals with xenografts, an increase in blood levels of prothrombotic metabolites activates AHR signaling within endothelial cells of large veins. AHR activation results in its nuclear translocation and the upregulation of TF and PAI-1 within endothelial cells. Both of these events are known to augment thrombogenesis and inhibit thrombolysis. In concert, this axis may contribute to cancer-associated VTE.

no correlation between the IVC clot weights, an indicator of venous thrombogenicity in mice, and the tumor mass (Figure 1D). Although this apparent discordance may be due to a smaller sample size or confounded by a rapid tumor growth, there is an alternative and potentially hypothesis-generating explanation. Malignancy exploits multiple ways to mediate VTE. Although it is conceivable that some of the mediators secreted by the tumors are dependent on tumor mass, it is also plausible that others, such as IS and Kyn, are influenced by the metabolism of the tumor. Recent studies have indicated that the metabolic rate of cancer cells is heterogeneous in a tumor and may not correlate linearly with the tumor mass.[46,47] In that case, the kinetics of a specific pathway within the tumor cells, rather than tumor mass per se, may govern the levels of these mediators. This notion may be further supported in colon cancer in humans. The higher tumor stage, as reflected by the TNM classification, suggests a greater tumor burden in humans. The "T" in the TNM classification is generally captured by the tumor size.[45,48] However, the TNM classification proposed by the National Comprehensive Cancer Network guideline for colon cancer does not include tumor size but rather is based on the invasiveness of the tumor. Further studies are needed to examine the effect of factors other than tumor mass on cancer-associated VTE.

AHR-TF/PAI-1 axis in cancer-associated VTE

Emerging evidence implicates the role of the AHR pathway in thrombosis through several mechanisms.[10-13] In endothelial cells, AHR activation increases TF messenger RNA, protects TF from ubiquitination and proteasomal degradation, and enhances the release of TF-bearing microvesicles. In essence, AHR activation can transform the endothelial cells from an anticoagulant surface to a procoagulant surface, enhancing thrombosis. IS is also known to increase platelet aggregation and adhesion, thereby augmenting thrombus formation.[49] Traditionally, platelets have remained a focus of arterial thrombosis. However, because antiplatelet agents are used successfully in the prevention of VTE,[50] it may suggest their role in cancer-associated DVT. The current study does not rule out the contribution of factors other than metabolites, such as inflammation, which are known to activate both AHR and TF signaling.[51,52]

AHR regulation of PAI-1 may be relevant in cancer-associated VTE. PAI-1 is the physiologic inhibitor of fibrinolysis and elicits its function by binding to and specifically inhibiting tissue plasminogen activator and urokinase plasminogen activator. An AHR-dependent increase in PAI-1 is noted in both Kyn-treated endothelial cell lysates and in the plasma of xenograft-bearing animals. This scenario provides evidence that AHR regulates PAI-1 in endothelial cells. These observations are consistent with that of Son et al,[16] who described PAI-1 as a transcriptional target of the AHR pathway in hepatoma cells. Our findings are relevant, as patients with different malignancies have higher levels of PAI-1.[53,54] Overall, the current study suggests the AHR-TF/PAI-1 axis as a candidate mediator of colon cancer–associated VTE.

Translational potential of AHR-TF axis in cancer-associated VTE

In addition to its pathogenicity, the metabolite AHR-TF axis may have prognostic significance in cancer-associated VTE. Currently, available risk scores of VTE, such as the Khorana score and its modifications, are derived from limited numbers of subjects and include only a handful of variables. Thus, their ability to capture the staggering variability in patient- and cancer-related VTE risk[55,56] is suboptimal, as these scores cannot be generalized to some major cancer types.[57] Because the incidence of VTE varies according to cancer type, it suggests that cancer-specific thrombotic mediators play an important role. Thus, development of cancer-specific risk models for the prediction of VTE is needed to help guide targeted thromboprophylaxis.[58]

This pathway has features that may make it conducive to biomarker research. First, the nodes of this axis are quantifiable with high accuracy and in a scalable manner. For example,

metabolites can be measured in blood with sensitive and accurate methods, such as LC/MS.[32] Second, high-throughput assays with a wide dynamic range and optimized signal-to-noise ratio are also available to monitor the ability of serum to activate AHR and TF activity in endothelial cells. A recent study examined the nodes of the metabolite AHR-TF axis and correlated them with the thrombosis in patients with normal kidney function and chronic kidney disease.[13] In both these cohorts, with the use of unsupervised machine learning techniques, the levels of metabolites and potency of patients' sera to activate AHR pathway and TF in endothelial cells were sufficient to discriminate patients who subsequently developed thrombosis. A similar strategy can be envisioned for VTE risk stratification in patients with cancer.

AHR signaling may be an appealing target for cancer-associated VTE. The AHR pathway is implicated in the pathogenesis of different malignancies.[18] Using tool compounds, our laboratory and others have shown the pharmacological targetability of AHR protein.[15,26] Now that the current data support its role in cancer-associated VTE, AHR antagonists may fulfill a dual purpose in patients with malignancy. AHR is activated by endogenous ligands, such as 6-formylindolo[3,2-b]carbazole,[59] and also exogenous ligands such as environmental toxins. Ligands such as 6-formylindolo[3,2-b]carbazole maintain low levels of AHR activity in cells and drive basal levels of downstream AHR targets such as TF. This notion is supported by the fact that mice without xenografts had 5.2 $\pm$ 1.62% endothelial cells positive for nuclear AHR in IVC (Figure 4C). CH223191 is a potent competitive AHR inhibitor that suppresses the AHR pathway activated by endogenous ligands, as well as those ligands overproduced as part of the disease process, such as IS and Kyn. This may explain suppression of AHR targets by CH223191 below control levels (Figures 6E and 7F). Similar observations were noted in the arterial thrombosis model in which 2 discrete AHR antagonists, CB7993113 and CH223191, suppressed TF below basal levels in cultured vSMCs.[10,11] Furthermore, AHR antagonists do not directly target coagulation factors that constitute the hemostatic protective barrier and accordingly are expected to have lower bleeding risk.[11]

Inherent in a mouse study are a few limitations. The allogenic xenografts mandate the use of immunocompromised mice such as athymic nude mice. Such a model will be devoid of components of immunity in thrombus formation, which limits the ability to probe for the role of innate immunity in thrombosis "immunothrombosis,"[60] likely a focus of other investigations. Although the current study used the xenograft model, tumors in their natural environment (orthotropic models) are more representative of human tumors. The aforementioned limitations can be addressed in future studies with the use of humanized mice or syngeneic orthotropic models.

In an era of precision medicine, cancer-associated thrombosis can be a predictable and preventable event. Addressing this unmet need warrants mechanistic probing of translationally relevant animal models. Although unbiased omics approaches are underway, a hypothesis-driven study of mediators, as illustrated in the current work, provides unique mechanistic insights. The translational potential of these findings is underscored by the fact that the components of the metabolite AHR-TF/PAI-1 axis can potentially be leveraged to individualize the risk prediction for cancer-associated thrombosis, as done in other human diseases,[13] and therapeutically targeted to improve the management of at-risk cancer patients.

Acknowledgments

The authors thank Brian Cooley (University of North Carolina at Chapel Hill) for guiding the development of the IVC occlusion model. They acknowledge Nader Rahimi (BUSM) for providing endothelial cell lines and David Sherr (BUSM) for establishing the AHR activity assay. They also acknowledge the Boston University Chemical Instrumentation Core for performing the metabolomics study. They thank Michael Kirber at the BUMC Core facilities for his assistance in confocal microscopy and calculation of integrated density values. They appreciate the technical assistance of Joseph Tashjian and Irva Vellard (BUSM) in IHC and immunoblotting and Elysia Heilig, Saran Lotfollahzadeh, and Ariearavanan Chinnappan (BUSM) for reviewing the manuscript.

This work was funded in part by the National Institutes of Health (National Heart, Lung, and Blood Institute, R01HL132325; National Cancer Institute, R01CA175382), Evans Faculty Merit award (V.C.C.), National Heart, Lung, and Blood Institute, National Institutes of Health (R01HL080442 and R01HL136363, K.R.), T32 training grant in cardiovascular biology T32 HL007224-40 (J.W.) and immunobiology of Trauma T32 GM86308 (N.A.) and Renal T32 DK007053-44 (C.L.). A part of this work was funded by the Thrombosis and Hemostasis in Health and Disease Affinity Research Collaborative program from the Department of Medicine of BUSM.

Authorship

Contribution: V.C.C., M.B., and K.R. designed the research and experiments; M.A.N., S.R., D.R., J.W., N.A., J.M.F., W.Y., C.L., and C.T. performed the cell-based studies; M.B. and D.R. performed immunofluorescence studies; M.B., D.R., J.W., W.Y., and S.R. performed the animal experiments; S.A.W. and N.L. performed the metabolomics study for Kyn and IS levels; V.C.C. and M.B. reviewed and analyzed the final data; M.B. and V.C.C. prepared the figures and manuscript; and C.S., C.A., and K.R. contributed conceptually to different degrees and edited the manuscript.

Conflict-of-interest disclosure: The authors declare no competing financial interests.

ORCID profiles: M.B., 0000-0002-2097-6882; M.A.N., 0000-0003-1879-7567; S.A.W., 0000-0002-5439-6501; V.C.C., 0000-0002-6663-6058.

Correspondence: Vipul C. Chitalia, Department of Medicine, Boston University Medical Center, Evans Biomedical Research Center, X-530, Boston, MA 02118; e-mail: vichital@bu.edu, vipul.chitalia@va.gov.

Footnotes

Submitted 20 May 2019; accepted 17 October 2019. Prepublished online as *Blood* First Edition paper, 5 November 2019; DOI 10.1182/blood.2019001675.

A portion of this work was accepted at an oral presentation at the 2018 American Society of Hematology meeting in San Diego, CA, 1-4 December 2018.

All data-sharing requests should be sent to the corresponding author, Vipul C. Chitalia (e-mail: vichital@bu.edu, vipul.chitalia@va.gov).

The online version of this article contains a data supplement.

There is a *Blood* Commentary on this article in this issue.

The publication costs of this article were defrayed in part by page charge payment. Therefore, and solely to indicate this fact, this article is hereby marked "advertisement" in accordance with 18 USC section 1734.

REFERENCES

1. Hisada Y, Mackman N. Cancer-associated pathways and biomarkers of venous thrombosis. *Blood*. 2017;130(13):1499-1506.
2. Heit JA, O'Fallon WM, Petterson TM, et al. Relative impact of risk factors for deep vein thrombosis and pulmonary embolism: a population-based study. *Arch Intern Med*. 2002;162(11):1245-1248.
3. Blom JW, Vanderschoot JP, Oostindiër MJ, Osanto S, van der Meer FJ, Rosendaal FR. Incidence of venous thrombosis in a large cohort of 66,329 cancer patients: results of a record linkage study. *J Thromb Haemost*. 2006;4(3):529-535.
4. Khorana AA, Francis CW, Culakova E, Kuderer NM, Lyman GH. Frequency, risk factors, and trends for venous thromboembolism among hospitalized cancer patients. *Cancer*. 2007; 110(10):2339-2346.
5. Stein PD, Beemath A, Meyers FA, Skaf E, Sanchez J, Olson RE. Incidence of venous thromboembolism in patients hospitalized with cancer. *Am J Med*. 2006;119(1):60-68.
6. Levitan N, Dowlati A, Remick SC, et al. Rates of initial and recurrent thromboembolic disease among patients with malignancy versus those without malignancy. Risk analysis using Medicare claims data. *Medicine (Baltimore)*. 1999;78(5):285-291.
7. Khorana AA, Francis CW, Culakova E, Kuderer NM, Lyman GH. Thromboembolism is a leading cause of death in cancer patients receiving outpatient chemotherapy. *J Thromb Haemost*. 2007;5(3):632-634.
8. White RH, Chew H, Wun T. Targeting patients for anticoagulant prophylaxis trials in patients with cancer: who is at highest risk? *Thromb Res*. 2007;120(suppl 2):S29-S40.
9. Chen N, Ren M, Li R, et al. Bevacizumab promotes venous thromboembolism through the induction of PAI-1 in a mouse xenograft model of human lung carcinoma. *Mol Cancer*. 2015;14(1):140.
10. Chitalia VC, Shivanna S, Martorell J, et al. Uremic serum and solutes increase post-vascular interventional thrombotic risk through altered stability of smooth muscle cell tissue factor. *Circulation*. 2013;127(3): 365-376.
11. Shashar M, Belghasem ME, Matsuura S, et al. Targeting STUB1-tissue factor axis normalizes hyperthrombotic uremic phenotype without increasing bleeding risk. *Sci Transl Med*. 2017; 9(417):
12. Gondouin B, Cerini C, Dou L, et al. Indolic uremic solutes increase tissue factor production in endothelial cells by the aryl hydrocarbon receptor pathway. *Kidney Int*. 2013;84(4):733-744.
13. Kolachalama VB, Shashar M, Alousi F, et al. Uremic solute-aryl hydrocarbon receptor-tissue factor axis associates with thrombosis after vascular injury in humans. *J Am Soc Nephrol*. 2018;29(3):1063-1072.
14. Shashar M, Francis J, Chitalia V. Thrombosis in the uremic milieu—emerging role of "thrombolome". *Semin Dial*. 2015;28(2): 198-205.
15. Shivanna S, Kolandaivelu K, Shashar M, et al. The Aryl hydrocarbon receptor is a critical regulator of tissue factor stability and an antithrombotic target in uremia. *J Am Soc Nephrol*. 2016;27(1):189-201.
16. Son DS, Rozman KK. 2,3,7,8-Tetrachlorodibenzo-p-dioxin (TCDD) induces plasminogen activator inhibitor-1 through an aryl hydrocarbon receptor-mediated pathway in mouse hepatoma cell lines. *Arch Toxicol*. 2002;76(7):404-413.
17. Wang F, Shi S, Zhang R, Hankinson O. Identifying target genes of the aryl hydrocarbon receptor nuclear translocator (Arnt) using DNA microarray analysis. *Biol Chem*. 2006;387(9):1215-1218.
18. Murray IA, Patterson AD, Perdew GH. Aryl hydrocarbon receptor ligands in cancer: friend and foe. *Nat Rev Cancer*. 2014;14(12): 801-814.
19. Suzuki Y, Suda T, Furuhashi K, et al. Increased serum kynurenine/tryptophan ratio correlates with disease progression in lung cancer. *Lung Cancer*. 2010;67(3):361-365.
20. Zhai L, Dey M, Lauing KL, et al. The kynurenine to tryptophan ratio as a prognostic tool for glioblastoma patients enrolling in immunotherapy. *J Clin Neurosci*. 2015;22(12): 1964-1968.
21. de Jong RA, Nijman HW, Boezen HM, et al. Serum tryptophan and kynurenine concentrations as parameters for indoleamine 2,3-dioxygenase activity in patients with endometrial, ovarian, and vulvar cancer. *Int J Gynecol Cancer*. 2011;21(7):1320-1327.
22. Uno K, Homma S, Satoh T, et al. Tissue factor expression as a possible determinant of thromboembolism in ovarian cancer. *Br J Cancer*. 2007;96(2):290-295.
23. Puccetti P, Fallarino F, Italiano A, et al. Accumulation of an endogenous tryptophan-derived metabolite in colorectal and breast cancers. *PLoS One*. 2015;10(4):e0122046.
24. Engin AB, Karahalil B, Karakaya AE, Engin A. Helicobacter pylori and serum kynurenine-tryptophan ratio in patients with colorectal cancer. *World J Gastroenterol*. 2015;21(12): 3636-3643.
25. Wolf H, Brown RR, Nyholm K. Studies on tryptophan metabolism in Danish bladder cancer patients. *Acta Vitaminol Enzymol*. 1975;29(1-6):117-122.
26. Chung KT, Gadupudi GS. Possible roles of excess tryptophan metabolites in cancer. *Environ Mol Mutagen*. 2011;52(2):81-104.
27. Pichler R, Fritz J, Heidegger I, et al. Predictive and prognostic role of serum neopterin and tryptophan breakdown in prostate cancer. *Cancer Sci*. 2017;108(4):663-670.
28. Shashar M, Siwak J, Tapan U, et al. c-Cbl mediates the degradation of tumorigenic nuclear β-catenin contributing to the heterogeneity in Wnt activity in colorectal tumors. *Oncotarget*. 2016;7(44):71136-71150.
29. Wang JG, Geddings JE, Aleman MM, et al. Tumor-derived tissue factor activates coagulation and enhances thrombosis in a mouse xenograft model of human pancreatic cancer. *Blood*. 2012;119(23):5543-5552.
30. Hiles LCA, Palmer O, Emamdjomeh A, et al. Impact of solid tumors on venous thrombosis: a novel unified model to understand cancer-associated thrombosis. *Circulation*. 2018; 134(suppl 1):20227.
31. Diaz JA, Obi AT, Myers DD Jr., et al. Critical review of mouse models of venous thrombosis. *Arterioscler Thromb Vasc Biol*. 2012; 32(3):556-562.
32. Zhang A, Rijal K, Ng SK, Ravid K, Chitalia V. A mass spectrometric method for quantification of tryptophan-derived uremic solutes in human serum. *J Biol Methods*. 2017;4(3):e75.
33. Chantrathammachart P, Mackman N, Sparkenbaugh E, et al. Tissue factor promotes activation of coagulation and inflammation in a mouse model of sickle cell disease. *Blood*. 2012;120(3):636-646.
34. Luyendyk JP, Cantor GH, Kirchhofer D, Mackman N, Copple BL, Wang R. Tissue factor-dependent coagulation contributes to alpha-naphthylisothiocyanate-induced cholestatic liver injury in mice. *Am J Physiol Gastrointest Liver Physiol*. 2009;296(4): G840-G849.
35. Zuo H, Ueland PM, Ulvik A, et al. Plasma biomarkers of inflammation, the kynurenine pathway, and risks of all-cause, cancer, and cardiovascular disease mortality: the Hordaland Health Study. *Am J Epidemiol*. 2016; 183(4):249-258.
36. Mackman N. Triggers, targets and treatments for thrombosis. *Nature*. 2008;451(7181): 914-918.
37. Day SM, Reeve JL, Pedersen B, et al. Macrovascular thrombosis is driven by tissue factor derived primarily from the blood vessel wall. *Blood*. 2005;105(1):192-198.
38. Walczak K, Dąbrowski W, Langner E, et al. Kynurenic acid synthesis and kynurenine aminotransferases expression in colon derived normal and cancer cells. *Scand J Gastroenterol*. 2011;46(7-8):903-912.
39. Qi Y, Wang R, Zhao L, et al. Celastrol suppresses tryptophan catabolism in human colon cancer cells as revealed by metabolic profiling and targeted metabolite analysis. *Biol Pharm Bull*. 2018;41(8):1243-1250.
40. Fan TW, El-Amouri SS, Macedo JKA, et al. Stable isotope-resolved metabolomics shows metabolic resistance to anti-cancer selenite in 3D spheroids versus 2D cell cultures. *Metabolites*. 2018;8(3):E40.
41. Riedl A, Schlederer M, Pudelko K, et al. Comparison of cancer cells in 2D vs 3D culture reveals differences in AKT-mTOR-S6K signaling and drug responses. *J Cell Sci*. 2017; 130(1):203-218.
42. Chen L, Tai WC, Brar MS, Leung FC, Hsiao WL. Tumor grafting induces changes of gut microbiota in athymic nude mice in the presence and absence of medicinal Gynostemma saponins. *PLoS One*. 2015; 10(5):e0126807.
43. Sobhani I, Tap J, Roudot-Thoraval F, et al. Microbial dysbiosis in colorectal cancer (CRC) patients. *PLoS One*. 2011;6(1):e16393.
44. Zackular JP, Baxter NT, Iverson KD, et al. The gut microbiome modulates colon tumorigenesis. *MBio*. 2013;4(6):e00692-e13.

45. Khorana AA, McCrae KR. Risk stratification strategies for cancer-associated thrombosis: an update. *Thromb Res*. 2014;133(suppl 2): S35-S38.

46. Sun C, Li T, Song X, et al. Spatially resolved metabolomics to discover tumor-associated metabolic alterations. *Proc Natl Acad Sci U S A*. 2019;116(1):52-57.

47. Vander Heiden MG, DeBerardinis RJ. Understanding the Intersections between Metabolism and Cancer Biology. *Cell*. 2017; 168(4):657-669.

48. Furie B, Furie BC. Cancer-associated thrombosis. *Blood Cells Mol Dis*. 2006;36(2): 177-181.

49. Yang K, Du C, Wang X, et al. Indoxyl sulfate induces platelet hyperactivity and contributes to chronic kidney disease-associated thrombosis in mice. *Blood*. 2017;129(19): 2667-2679.

50. Becattini C, Agnelli G. Aspirin for prevention and treatment of venous thromboembolism. *Blood Rev*. 2014;28(3):103-108.

51. Steffel J, Lüscher TF, Tanner FC. Tissue factor in cardiovascular diseases: molecular mechanisms and clinical implications. *Circulation*. 2006;113(5):722-731.

52. Vondrácek J, Umannová L, Machala M. Interactions of the aryl hydrocarbon receptor with inflammatory mediators: beyond CYP1A regulation. *Curr Drug Metab*. 2011;12(2): 89-103.

53. McMahon B, Kwaan HC. The plasminogen activator system and cancer. *Pathophysiol Haemost Thromb*. 2008;36(3-4):184-194.

54. Placencio VR, DeClerck YA. Plasminogen activator inhibitor-1 in cancer: rationale and insight for future therapeutic testing. *Cancer Res*. 2015;75(15):2969-2974.

55. Lyman GH, Khorana AA, Kuderer NM, et al; American Society of Clinical Oncology Clinical Practice. Venous thromboembolism prophylaxis and treatment in patients with cancer: American Society of Clinical Oncology clinical practice guideline update. *J Clin Oncol*. 2013; 31(17):2189-2204.

56. Ay C, Dunkler D, Marosi C, et al. Prediction of venous thromboembolism in cancer patients. *Blood*. 2010;116(24):5377-5382.

57. Santi RM, Ceccarelli M, Catania G, et al. PO-03—Khorana score and histotype predict the incidence of early venous thromboembolism (VTE) in Non Hodgkin Lymphoma (NHL). A pooled data analysis of twelve clinical trials of Fondazione Italiana Linfomi (FIL). *Thromb Res*. 2016;140(suppl 1):S177.

58. Noble S, Alikhan R, Robbins A, Macbeth F, Hood K. Predictors of active cancer thromboembolic outcomes: validation of the Khorana score among patients with lung cancer: comment. *J Thromb Haemost*. 2017;15(3): 590-591.

59. Stejskalova L, Dvorak Z, Pavek P. Endogenous and exogenous ligands of aryl hydrocarbon receptor: current state of art. *Curr Drug Metab*. 2011;12(2):198-212.

60. Grover SP, Mackman N. Neutrophils, NETs, and immunothrombosis. *Blood*. 2018;132(13): 1360-1361.